HHS Public Access

Author manuscript

Dig Dis Sci. Author manuscript; available in PMC 2023 March 15.

Published in final edited form as:

Dig Dis Sci. 2022 October ; 67(10): 4805–4812. doi:10.1007/s10620-021-07372-w.

Esophageal OCT imaging using a paddle probe externally attached to endoscope

Kengyeh K. Chu[1], **Yang Zhao**[1], **Evan T. Jelly**[1], **Zachary A. Steelman**[1], **Michael Crose**[1], **Brian Cox**[1], **Yaa Ofori-Marfoh**[2], **Lama Moussa**[2], **Holly Cirri**[2], **Ariel Watts**[2], **Nicholas Shaheen**[2], **Adam Wax**[1]

[1]Dept. of Biomedical Engineering, Duke University, Durham, NC

[2]Center for Esophageal Diseases and Swallowing, University of North Carolina, Chapel Hill, NC

Abstract

Background and Aims—Endoscopic surveillance of Barrett's esophagus (BE) by white light examination is insufficient to diagnose dysplastic change. In this work, we describe an optical imaging method to obtain high-resolution cross-sectional imaging using a paddle-shaped probe affixed to the endoscope tip.

Methods—We integrated Optical Coherence Tomography (OCT), an optical imaging method that produces cross-sectional images, into a paddle probe attached to video endoscope. We acquired images of esophageal epithelium from patients undergoing routine upper GI endoscopy. Images were classified by a reviewer blinded to patient identity and condition, and these results were compared with clinical diagnosis.

Results—We successfully captured epithelial OCT images from 30 patients and identified features consistent with both squamous epithelium and Barrett's esophagus. Our blinded image reviewer classified BE vs. non-BE with 91.5% accuracy (65/71 image regions), including sensitivity of 84.6% for BE (11/13) and a specificity of 93.1% (54/58). However, in 16 patients, intubation of the probe into the esophagus could not be achieved.

Conclusions—A paddle probe is a feasible imaging format for acquiring cross-sectional OCT images from the esophagus, and can provide a structural assessment of BE and non-BE tissue. Probe form factor is the current limiting obstacle, but could be addressed by further miniaturization.

Keywords

Optical coherence tomography; Barrett's esophagus; new technology; imaging

Introduction

Esophageal cancer was responsible for 17,290 deaths in the United States in 2018 [1], remaining one of the leading causes of cancer death nationally. The recent trend of death rates from esophageal cancer in the US is on the decline, likely due to an increasing emphasis on early detection and the timely treatment of early cancers [2], but incidence of esophageal adenocarcinoma (EAC) has continued to rise [3]. The only known precursor to EAC is Barrett's esophagus (BE), a metaplastic transformation of squamous esophageal

epithelium to columnar epithelium with goblet cells. BE is thought to be a sequelae of gastric reflux, and is associated with increased risk of developing EAC [4]. BE patients are managed using guidelines for the surveillance and treatment of patients at risk for and diagnosed with BE [5].

Following a diagnosis of non-dysplastic BE, a patient is usually referred for periodic endoscopic surveillance to monitor the esophagus for progression to dysplasia. During each endoscopic procedure, the presence of dysplasia is determined by biopsy, typically following a systematic sampling pattern prescribed in the Seattle protocol [6, 7]. Adherence to this protocol can become a substantial burden in the long term due to the many biopsies that may be required while providing only a relatively sparse sampling of the region of tissue at risk of metaplasia and dysplasia [8]. Sensitive detection and diagnosis of dysplasia *in situ* would maximize efficiency, by allowing both a diagnostic surveillance exam as well as a therapeutic treatment at the same session, using modalities such as radiofrequency ablation (RFA) [9], which might be integrated into the same paddle as the imaging technology.

Noninvasive optical volumetric imaging of the esophageal mucosa is therefore an attractive option for surveillance of BE. One such method is optical coherence tomography (OCT) [10], a technique that uses infrared light to form cross-sectional images of esophageal epithelium [11, 12]. OCT can sensitively and comprehensively detect surface and subsurface markers of BE and dysplasia that are not detectable from a video endoscopy [13]. Compared to confocal microendoscopy [14, 15], which can also offer microscopic images of the esophagus, OCT reveals subsurface structure across the full thickness of the epithelium and does not require contrast agents.

Approaches that measure the scattering of light rather than directly imaging the tissue have also been developed [16]. For BE, discrimination of dysplasia is based on identifying the scattering profiles of the enlarged nuclei that are characteristic of dysplasia [17]. One implementation that measures the spectral signature of enlarged nuclei is termed multispectral light scattering [18, 19]. Our group has also developed angle-resolved low coherence interferometry (a/LCI), a technique that distinguishes the scattering signatures of dysplastic and non-dysplastic nuclei [20, 21]. a/LCI has demonstrated high sensitivity and specificity for dysplasia in BE [19], but is limited to a relatively narrow field of less than 1 mm. These scattering methods provide quantitative metrics that serve as unique biomarkers for dysplasia, but lack the structural context of 3D imaging, and do not allow the scanning of larger areas of mucosa, a strength of OCT.

OCT probes capable of accessing the esophageal lumen have been developed in several forms. One such format is a rotating fiber optic probe centered within an inflated balloon, inserted into the esophagus with the aid of an endoscope [22]. Another type of probe allows the patient to swallow a pill-like transparent capsule containing a similar rotating fiber optic, employing peristalsis to advance the probe through the esophagus and into the stomach [23].

In our present work, we aimed to develop a new probe format that could be more easily adapted to a “see-and-treat” workflow during surveillance endoscopy. This probe consists of a paddle-like housing that attaches to the tip of the endoscope, similar in shape to a

focal RFA treatment paddle. While the main goal of our current work was to establish the feasibility of performing targeted OCT imaging of the esophageal epithelium during an endoscopic exam using the paddle form, we also evaluated the adaptability of our approach to allow the future addition of the a/LCI modality to the current OCT imaging by implementing a paddle design that included a placeholder chamber and window based on a preliminary a/LCI optical design. Such a conformation might allow OCT as an initial “red flag” imaging, with a/LCI utilized to provide a more detailed analysis of possible dysplasia.

Methods

Optical Coherence Tomography (OCT)

We used OCT to provide cross-sectional images of the esophageal epithelium. The technical details of the system are provided below. Briefly, an OCT system illuminates a sample with a beam of light. The depths of all reflections from a sample are determined using interferometry to produce a depth profile. Depth profiles are compiled into images by scanning the location of the beam on the sample, producing a 2D image in a manner similar to ultrasound.

Fiber optics contained in a custom sheath and paddle assembly were attached to an upper GI endoscope. A steel cable within the sheath turned the optical fiber assembly to produce images. Our OCT interferometric instrumentation was contained in a portable steel cart.

OCT probe paddle housing

The probe was paddle-shaped and designed to be attached to the tip of the endoscope (Figure 1.) The housing was 3D printed using a biocompatible dental-grade resin (FormLabs, Somerville, MA). A flexible cuff for attachment to the endoscope was 3D printed using silicone (Carbon 3D, Redwood City, CA). An anti-reflective rectangular sapphire optical window (Guild Optics, Amherst, NH) was attached to the paddle. Biocompatible silicone (Masterbond, Hackensack, NJ) was applied to seal seams between components.

During the course of the study, three versions of the paddle were created (Figure 1). Initially (Fig. 1A), the paddle was symmetric and included a tapered shape to facilitate articulation. In the subsequent design (Fig. 1B), modified in response to feedback from the endoscopist (NS), the front edge of the paddle was shortened and rounded to facilitate navigation of the probe through the upper esophageal sphincter (UES). The tapered shape at the proximal end of the paddle was deemed unnecessary, and was instead flattened to improve mechanical protection of the fiber optic probe within. In a final design iteration, we further revised the geometry of the probe to allow future use as a multimodality probe that would include additional optical elements to enable use of a/LCI. We reduced the thickness and increased the length of the probe, while placing the OCT optics off-center (Fig. 1C).

The fiber optic elements in the OCT probe were enclosed in an ETFE tube (Zeus, Orangeburg, SC) fixed to a threaded brass tubing connector and secured to a bulkhead.

Clinical imaging

Human subjects research was conducted with approval from the Institutional Review Boards at Duke University Health System (Pro0090173) and the University of North Carolina (17–3037).

Subjects were recruited from patients undergoing routine care endoscopy at UNC Healthcare. Patients between the ages of 18 and 80 years presenting for upper endoscopy were eligible if one of the following criteria was satisfied: 1) No history of gastroesophageal reflux disease (GERD) or other esophageal condition affecting the epithelium, and without esophageal symptomology (including heartburn, globus, chest pain, dysphagia, and odonophagia); 2) Current dysplastic or non-dysplastic Barrett's esophagus of any length; or 3) History of dysplastic or non-dysplastic Barrett's esophagus after successful treatment with endoscopic eradication therapy (EET). Exclusion criteria included prior esophageal surgery (excepting uncomplicated Nissen fundoplication), pregnancy, inability to provide written informed consent, and a history of esophageal stricture or prior esophageal dilation.

To begin an imaging session, the endoscopist placed the silicone cuff over the tip of the endoscope similar to the placement of a focal RFA catheter, and navigated the probe into the esophagus under video guidance. The tip of the paddle was visible in the video endoscopy field of view, and was used to visually guide the OCT imaging location. For subjects with suspected regions of Barrett's esophagus or dysplasia, at least one OCT scan was acquired by placing the imaging window against the abnormal tissue, and commencing an imaging sequence of 10 to 15 frames. For all subjects, at least one such OCT scan was also acquired from a region of apparently healthy squamous epithelium. Following imaging, the endoscope was withdrawn. If biopsies were acquired as part of the patient's medical care from imaged regions, pathology results were obtained and added to the patient's research record to classify tissue types.

Classification

Our ability to discern BE from OCT was evaluated by comparing the image-based classification made by a human reviewer with the clinical diagnosis based on the pathology reading from a biopsy at the same location where available. Squamous tissue was differentiated from BE by endoscopic appearance, and confirmed histologically by the presence of specialized metaplasia demonstrating goblet cells. In some cases (2 patients), a clinical biopsy was not obtained because immediate RFA rendered pre-treatment histology moot. In these cases, BE was classified based on visual findings consistent with BE and a previous history of histological samples demonstrating BE. 71 image sets were randomly ordered and presented to an OCT reader masked as to the clinical classification of the tissue, who classified the image sets into BE and normal categories. OCT interpretation was then compared to the clinical diagnosis and scored by its sensitivity and specificity to BE as well as overall classification accuracy.

OCT technical details

The OCT system was a spectral-domain fiber-optic Michelson interferometer design (Figure 2). Illumination was provided by a superluminescent diode (Exalos, Schlieren, Switzerland)

centered at 1318 nm with a −3 dB bandwidth of 83 nm. The sample arm included a fiber-optic rotary junction (FORJ) (Princetel, Hamilton, NJ), which allowed rotation of the distal optics within the probe while remaining optically coupled to the stationary proximal sample arm. The FORJ was rotated using a mechanical coupling driven by a stepper motor (Teknic, Victor, NY). Optical and mechanical connection to the probe was accomplished via a rectangular SC-APC connector, which effectively transmitted driving torque directly to the connector. The probe shaft was a three-layer wound steel torque coil (Asahi Intecc, Seto-shi, Japan) surrounding a SMF-28 fiber. Distal optics, including a gradient-index (GRIN) objective lens and a prism, produced a focused beam in a side-viewing configuration that enabled tissue imaging through the probe window.

Light returning from the probe was combined with reference light and detected using a custom spectrometer [24]. The spectrometer optics were modeled and optimized using optical design software (OpticsStudio, Radiant Zemax), and the physical components were designed using CAD software (Solidworks, Waltham, MA). The body of the spectrometer was 3D printed (Dremel 3D45) using Eco-ABS (Dremel, Racine, WI). The spectrometer sensor was an InGaAs linear array (Sensors Unlimited, Princeton, NJ).

OCT probe optics

The OCT probe consisted of a single-mode optical fiber enclosed within a steel torque coil that transmitted the driving force of the probe. Optical connector epoxy was applied to secure the coil to the connector body on the proximal end, and to the fiber ferrule on the distal end. Two optical probe designs were used in this study, starting with a custom GRIN assembly built in-house, and progressing to another custom fabricated GRIN design assembled by the GRIN manufacturer (GRINtech, Jena, Germany) (Figure 3).

In the first design, the distal optical fiber was terminated at a 1 mm glass ferrule (Accu-Glass, St. Louis, MO). The ferrule face was polished by clamping the ferrule into a bare fiber FC/APC adapter with a 1 mm bore and using a motorized fiber polisher (KrellTech, Neptune City, NJ), resulting in a reflection-minimizing 8-degree angle polish. The ferrule was then inserted into a steel hypotube segment with a small hole machined into its side. The GRIN objective lens was placed into the tube leaving 0.44 mm of space between the GRIN and the ferrule, a distance determined by optical modeling to achieve the desired working distance. The ferrule-GRIN gap was filled in with optical adhesive (Norland Products, Cranbury, NJ) for index matching. Finally, a right angle prism (Edmund Optics, Barrington, NJ) was attached to the GRIN with optical adhesive for a side-viewing configuration.

Despite the use of index matching optical adhesive between probe surfaces, there were still significant artifacts due to reflections in this first design. This limitation prompted an optical redesign during the clinical study. In the second design, a custom GRIN optical assembly was commissioned to be fabricated by GRINtech, with the prime objective of eliminating the gap between the ferrule and the GRIN. This was achieved by utilizing a GRIN element greater than 0.25 pitch in length, bringing the fiber illumination to a converging focus without need for a spacer. The factory-made elements also included an

additional angle-polished interface between the GRIN and the prism, further eliminating specular reflections within the probe.

Image processing

Standard spectral-domain OCT imaging techniques were employed to process raw interferometric data into 2D depth profiles (B-scans), including background subtraction, k-space interpolation, and dispersion compensation [25].

Because the OCT scan is rotational, the B-scans derived from our images were natively in polar coordinates. Non-uniform rotational distortion (NURD) [26] caused a non-constant angular velocity that required correction using a custom procedure. First, we identified 8 key positions on the polar B-scan. In cross-section, the walls of the paddle cavity and the surface of the tissue form a rectangle; four key positions are the centers of each side, and the remaining four are the corners of the rectangle. Then, we estimated the true angular position of each A-line by using spline interpolation with the identified A-line positions as inputs and the known angular positions of those corresponding landmarks as outputs. Finally, we shifted these A-lines to conform to a linear angular ramp, and interpolated the B-scans in the angular dimension to smoothly fill the gaps. The polar coordinate images were then remapped to rectilinear coordinates and cropped.

Results

We recruited 54 patients into the esophageal OCT imaging study. One patient was withdrawn due to inadvertent enrollment despite reporting an exclusionary symptom (heartburn). Of the 53 remaining, the probe was successfully navigated into the esophagus of 37 patients, of which 30 yielded adequate image sets, and 7 experienced technical failures. Table 1 below summarizes the patient enrollment.

Comparison of probe optics

The majority of data was obtained using our in-house designed and fabricated GRIN probe (22 imaged patients.) A representative image of squamous epithelium and Barrett's esophagus as visualized with this probe are shown in Figure 4. Although image quality was generally adequate, internal reflections within the probe resulted in several bright line artifacts in the cross-sectional images. We minimized the overlap of the reflection artifact on key features of the image where possible, but unpredictable shifts in the visualized location of the tissue did occasionally result in unavoidable obscuration of portions of the image by the artifact.

The second probe, designed with all angle-polished surfaces, substantially removed the reflection artifacts. The modified design was employed for the final eight patients imaged in this study. Representative images generated by this version of the probe are shown in Figure 5, which demonstrate the reduction in reflection artifacts.

Comparison of paddle probe designs

Our initial paddle design was utilized for only three patients, which were all successfully intubated, although only one resulted in usable images. Based on this experience with these cases, the clinician noted that a rounded front would be preferred for navigation past the UES to prevent catching on the sphincter. We therefore produced a second design that implemented a more snub-nose shaped, rounded anterior. Additionally, we noted that the degree of articulation permitted by the first design resulted in mechanical failures within the GRIN probe, which caused the technical failures in two of the three experiments. Our second design also incorporated a rigid metal hypotube segment to prevent excessive bending at the most vulnerable point of the optics.

The second paddle design was used for 23 imaging attempts, which resulted in 16 successful intubations (69.6%). The enhanced protection of this design prevented damage to the probes, and 13 successful imaging sessions. The third and final paddle design was used for 27 imaging attempts, 18 of which were successful intubations (66.7%), and 16 patients with successful image acquisitions.

Image classification

Table 2 shows the results of the classification of random-ordered deidentified OCT images by a reviewer compared with the clinical diagnosis.

The OCT classification of BE was 91.5% accurate overall (65/71 image regions). Sensitivity for BE was 84.6% for BE (11/13) and specificity was 93.1% (54/58).

Discussion

The primary aim in this work was to establish the feasibility of conducting OCT imaging of regions of esophageal epithelium selected by an endoscopist using a paddle probe mechanically coupled to the external housing of the endoscope. We were able to successfully image the majority of patients attempted and acquired high-resolution OCT images from the esophageal epithelium. Clear differences between squamous epithelium and Barrett’s esophagus were observed, demonstrating that paddle probe OCT can be an effective means of distinguishing these conditions. The penetration depth afforded by 1300 nm OCT enabled visualization of the epithelium, lamina propria, muscularis mucosa, and submucosa.

The paddle probe format suggested here can provide several advantages. First, an endoscopist can readily direct the imaging to a specific location during the endoscopic procedure, allowing quick imaging of a particular region of interest without requiring a full volumetric scan or the introduction of a new imaging probe during the procedure. Secondly, attaching the probe externally to the endoscope allows the instrument channel to remain free, such that other through-the-scope interventions are feasible. Thus, the endoscopist can readily image a region of interest and directly follow up with a biopsy without the need for exchanging instruments in the channel. Finally, a paddle format is amenable to future adaptation for multimodality imaging and treatment. The final probe used in this study demonstrated that we could maintain comparable performance in a paddle form factor that

included space to integrate a second optical modality, such as a/LCI. Additionally, this form factor was selected to allow potential implementation of a “see-and-treat” paradigm with endoscopic eradication therapy using the same paddle. Such an approach would enable the collapse of two episodes of care into a single endoscopy, and omit the costs associated with histological processing of biopsy specimens.

While our imaging approach does not provide a comprehensive volume image of the esophagus, the probe can be easily targeted to any region deemed suspect by the endoscopist, and can rapidly acquire images over multiple areas. Currently, this probe can be used to distinguish BE from squamous tissue by appearance on OCT. Classification accuracy using OCT was high overall, though possibly limited by the lack of exact registration between OCT scan locations and biopsy sites. While differentiation of squamous from BE tissue is not clinically relevant, as endoscopists can generally easily differentiate between the two, it does provide proof of principle that this side-viewing probe yields interpretable mucosal images. Additionally, although we did not assess the ability of our OCT device to differentiate dysplastic from non-dysplastic BE in this proof-of-principle study, previous work demonstrates that OCT has utility for this indication [27]. The qualitative features that distinguish these tissues may be recognized using artificial intelligence (AI) algorithms in the future.

Overall, imaging quality was very good, and imaging success rate was high after some initial mechanical failures of the optical probe. Reflection artifacts were substantially reduced using probes assembled by GRINtech, demonstrating the importance of angle-polishing of internal components joined by optical adhesive. This improvement was evident qualitatively, as image-disrupting reflections were visibly reduced.

Several key limitations should be discussed. The most important of these was that in approximately one third of cases, we could not pass the probe past the UES to perform esophageal imaging. While our success rate was adequate to demonstrate feasibility, further miniaturization of the probe components will be necessary to attain more universal success with intubation, especially in patients of small stature, those with scoliosis, and those with anterior cervical osteophytes. By limiting our inclusion criteria, we have also excluded pathologies other than BE that may add complexity to the current binary classification of BE vs. non-BE. Additionally, the bending of the probe sheath necessary to enter the esophagus caused uneven rotational friction that contributed to NURD. Though our processing was able to compensate for NURD, this added step was conducted manually at this point and thus was the rate-limiting component of the workflow. The development of real-time automated NURD correction would improve throughput. One potential solution for both miniaturization and NURD would be to replace the steel torque coil with a micromotor-driven mirror within the paddle.

This report documents the ongoing development process of this technology. We envision a single probe that will allow wider field OCT scanning, perhaps at multiple sites along a 2–3 cm paddle, used as a “red flag” technology, coupled with a/LCI imaging for higher accuracy of any lesions identified by the OCT scanning. Real-time AI algorithms would aid the endoscopist in interpretation of both the OCT and a/LCI scans. If adequate operating

characteristics could be achieved with such a system, the form function of the imaging device would allow housing of treatment elements, potentially including RFA or other thermal modalities. In this way, endoscopists performing surveillance procedures might both improve the accuracy of their exams over our current practice, and improve the efficiency of our approach by obviating the need for histological specimens and a second endoscopy to allow for treatment.

Acknowledgements

Support from NCI (R01-CA210544). Special thanks to Benjamin Goldberg for coding contributions. Special thanks to the lab of Dr. Ken Gall for 3D printing access.

Disclosures

AW is Founder and President of Lumedica, Inc. and Lumedica Vision. MC and BC are both currently employees and equity holders in Lumedica, Inc. and Lumedica Vision. ETJ is a graduate student intern with MicroElastic and is a consultant (non-financial) with Lumedica, Inc. NS has research funding from Interpace Diagnostics, Medtronic, Steris, Pentax, and CDx Medical and is a consultant for Cernostics, Cook Medical, Phathom, and Boston Scientific.

References

1. Siegel RL, Miller KD, and Jemal A, Cancer statistics, 2018. CA Cancer J Clin, 2018. 68(1): p. 7–30. [PubMed: 29313949]
2. Njei B, McCarty TR, and Birk JW, Trends in esophageal cancer survival in United States adults from 1973 to 2009: A SEER database analysis. J Gastroenterol Hepatol, 2016. 31(6): p. 1141–6. [PubMed: 26749521]
3. Hur C, et al. , Trends in esophageal adenocarcinoma incidence and mortality. Cancer, 2013. 119(6): p. 1149–58. [PubMed: 23303625]
4. Spechler SJ and Goyal RK, Barrett's esophagus. N Engl J Med, 1986. 315(6): p. 362–71. [PubMed: 2874485]
5. Shaheen NJ, et al. , ACG Clinical Guideline: Diagnosis and Management of Barrett's Esophagus. Am J Gastroenterol, 2016. 111(1): p. 30–50; quiz 51. [PubMed: 26526079]
6. Levine DS, et al. , An endoscopic biopsy protocol can differentiate high-grade dysplasia from early adenocarcinoma in Barrett's esophagus. Gastroenterology, 1993. 105(1): p. 40–50. [PubMed: 8514061]
7. Reid BJ, et al. , Optimizing endoscopic biopsy detection of early cancers in Barrett's high-grade dysplasia. The American journal of gastroenterology, 2000. 95(11): p. 3089–3096. [PubMed: 11095322]
8. Kariv R, et al. , The Seattle protocol does not more reliably predict the detection of cancer at the time of esophagectomy than a less intensive surveillance protocol. Clin Gastroenterol Hepatol, 2009. 7(6): p. 653–8; quiz 606. [PubMed: 19264576]
9. Shaheen NJ, et al. , Radiofrequency ablation in Barrett's esophagus with dysplasia. N Engl J Med, 2009. 360(22): p. 2277–88. [PubMed: 19474425]
10. Huang D, et al. , Optical coherence tomography. Science, 1991. 254(5035): p. 1178–81. [PubMed: 1957169]
11. Bouma BE, et al. , High-resolution imaging of the human esophagus and stomach in vivo using optical coherence tomography. Gastrointest Endosc, 2000. 51(4 Pt 1): p. 467–74. [PubMed: 10744824]
12. Vakoc BJ, et al. , Comprehensive esophageal microscopy by using optical frequency-domain imaging (with video). Gastrointest Endosc, 2007. 65(6): p. 898–905. [PubMed: 17383652]
13. Evans JA, et al. , Identifying intestinal metaplasia at the squamocolumnar junction by using optical coherence tomography. Gastrointest Endosc, 2007. 65(1): p. 50–6. [PubMed: 17137858]

14. Dunbar KB, et al. , Confocal laser endomicroscopy in Barrett's esophagus and endoscopically inapparent Barrett's neoplasia: a prospective, randomized, double-blind, controlled, crossover trial. Gastrointest Endosc, 2009. 70(4): p. 645–54. [PubMed: 19559419]
15. Kiesslich R, et al. , In vivo histology of Barrett's esophagus and associated neoplasia by confocal laser endomicroscopy. Clin Gastroenterol Hepatol, 2006. 4(8): p. 979–87. [PubMed: 16843068]
16. Steelman ZA, et al. , Light scattering methods for tissue diagnosis. Optica, 2019. 6(4): p. 479–489. [PubMed: 33043100]
17. Perelman LT, et al. , Observation of Periodic Fine Structure in Reflectance from Biological Tissue: A New Technique for Measuring Nuclear Size Distribution. Physical Review Letters, 1998. 80(3): p. 627–630.
18. Qiu L, et al. , Multispectral light scattering endoscopic imaging of esophageal precancer. Light Sci Appl, 2018. 7: p. 17174. [PubMed: 30839534]
19. Qiu L, et al. , Multispectral scanning during endoscopy guides biopsy of dysplasia in Barrett's esophagus. Nat Med, 2010. 16(5): p. 603–6, 1p following 606. [PubMed: 20383155]
20. Terry NG, et al. , Detection of dysplasia in Barrett's esophagus with in vivo depth-resolved nuclear morphology measurements. Gastroenterology, 2011. 140(1): p. 42–50. [PubMed: 20854820]
21. Wax A, et al. , Cellular organization and substructure measured using angle-resolved low-coherence interferometry. Biophysical journal, 2002. 82(4): p. 2256–2264. [PubMed: 11916880]
22. Suter MJ, et al. , Comprehensive microscopy of the esophagus in human patients with optical frequency domain imaging. Gastrointest Endosc, 2008. 68(4): p. 745–53. [PubMed: 18926183]
23. Gora MJ, et al. , Tethered capsule endomicroscopy enables less invasive imaging of gastrointestinal tract microstructure. Nat Med, 2013. 19(2): p. 238–40. [PubMed: 23314056]
24. Kim S, et al. , Design and implementation of a low-cost, portable OCT system. Biomed Opt Express, 2018. 9(3): p. 1232–1243. [PubMed: 29541516]
25. Wojtkowski M, et al. , Ultrahigh-resolution, high-speed, Fourier domain optical coherence tomography and methods for dispersion compensation. Optics express, 2004. 12(11): p. 2404–2422. [PubMed: 19475077]
26. Kimura BJ, et al. , Distortion of intravascular ultrasound images because of nonuniform angular velocity of mechanical-type transducers. American Heart Journal, 1996. 132(2, Part 1): p. 328–336. [PubMed: 8701894]
27. Struyvenberg M, et al. , Expert assessment on volumetric laser endomicroscopy full scans in Barrett's esophagus patients with or without high grade dysplasia or early cancer. Endoscopy, 2021. 53(3): p. 218–225. [PubMed: 32515006]

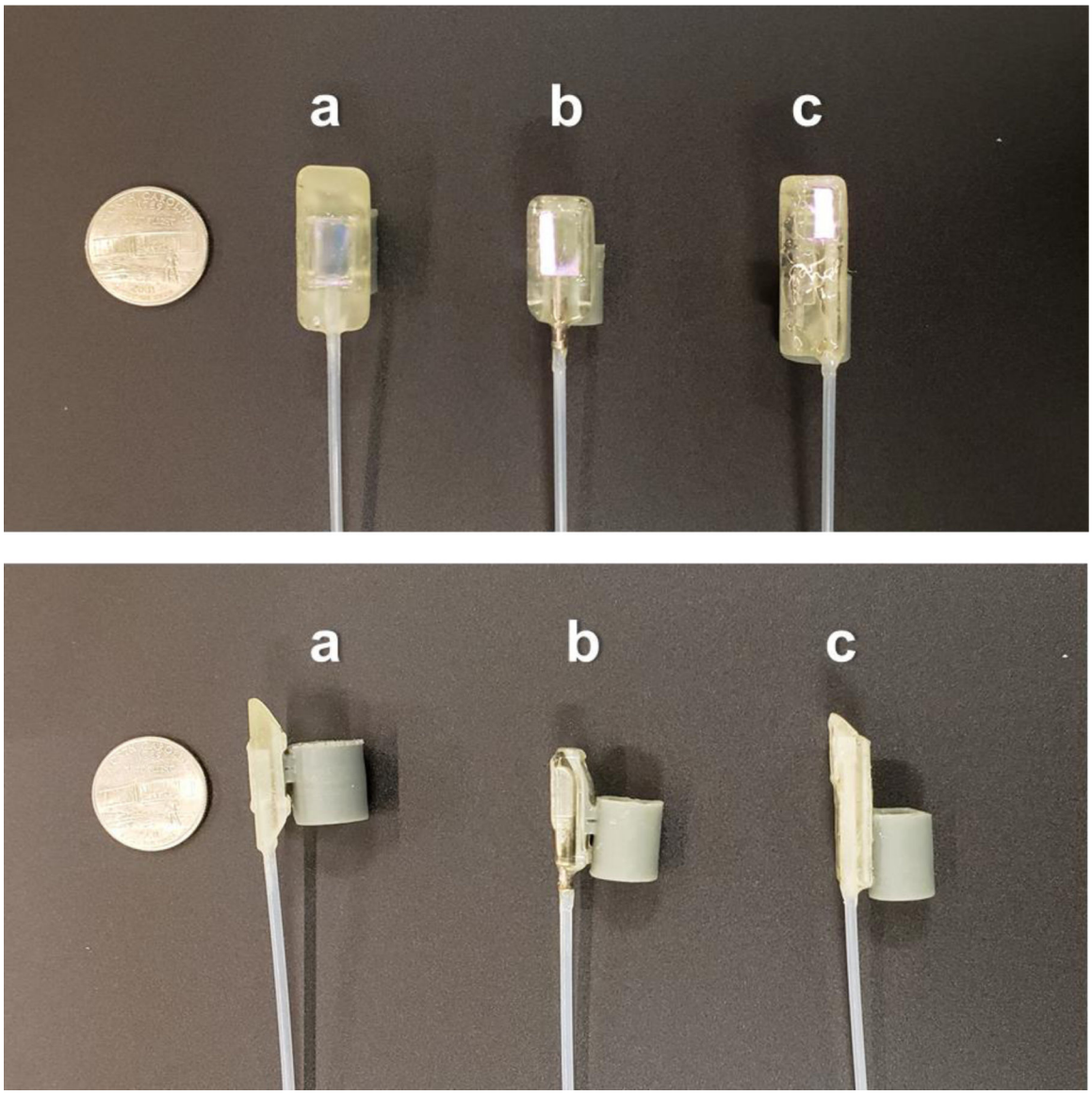

Figure 1:
Design iterations of the paddle probe housing with silicone cuff, showing top-down views (top) and lateral views (bottom). A) Initial design. B) Modified design with rounded front. C) Final design with extended rigid protection region, decreased profile height, and off-center placement of the OCT fiber to reserve space for a second modality. US quarter shown for scale (diameter = 24.3 mm)

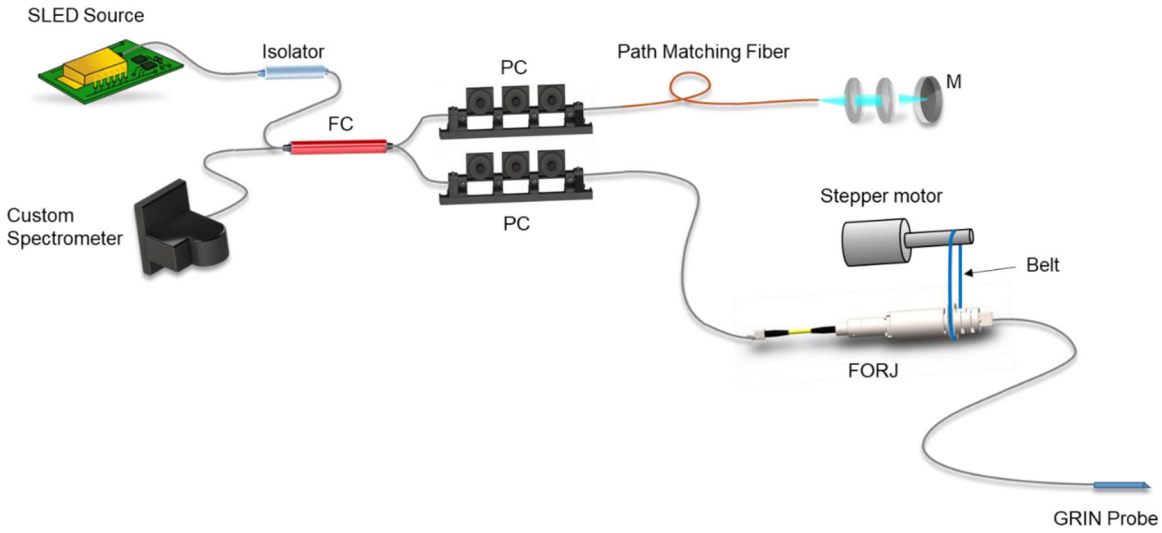

Figure 2:
Diagram of OCT fiber Michelson interferometer. SLED source: 1318 nm superluminescent diode. FC: Fiber coupler. PC: Polarization controller. M: Mirror. FORJ: Fiber optic rotary junction.

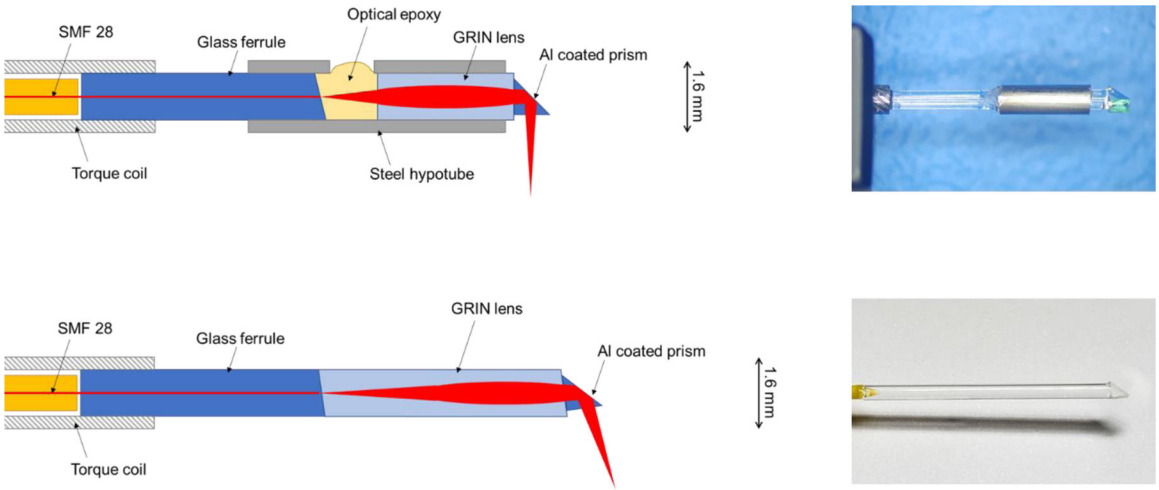

Figure 3:

First and second versions of side-viewing OCT probe optics. Top left: Diagram of probe optics, version 1. Top right: Photo of lab-assembled probe, version 1. Bottom left: Diagram of probe optics, version 2. Bottom right: Photo of factory-assembled probe, version 2.

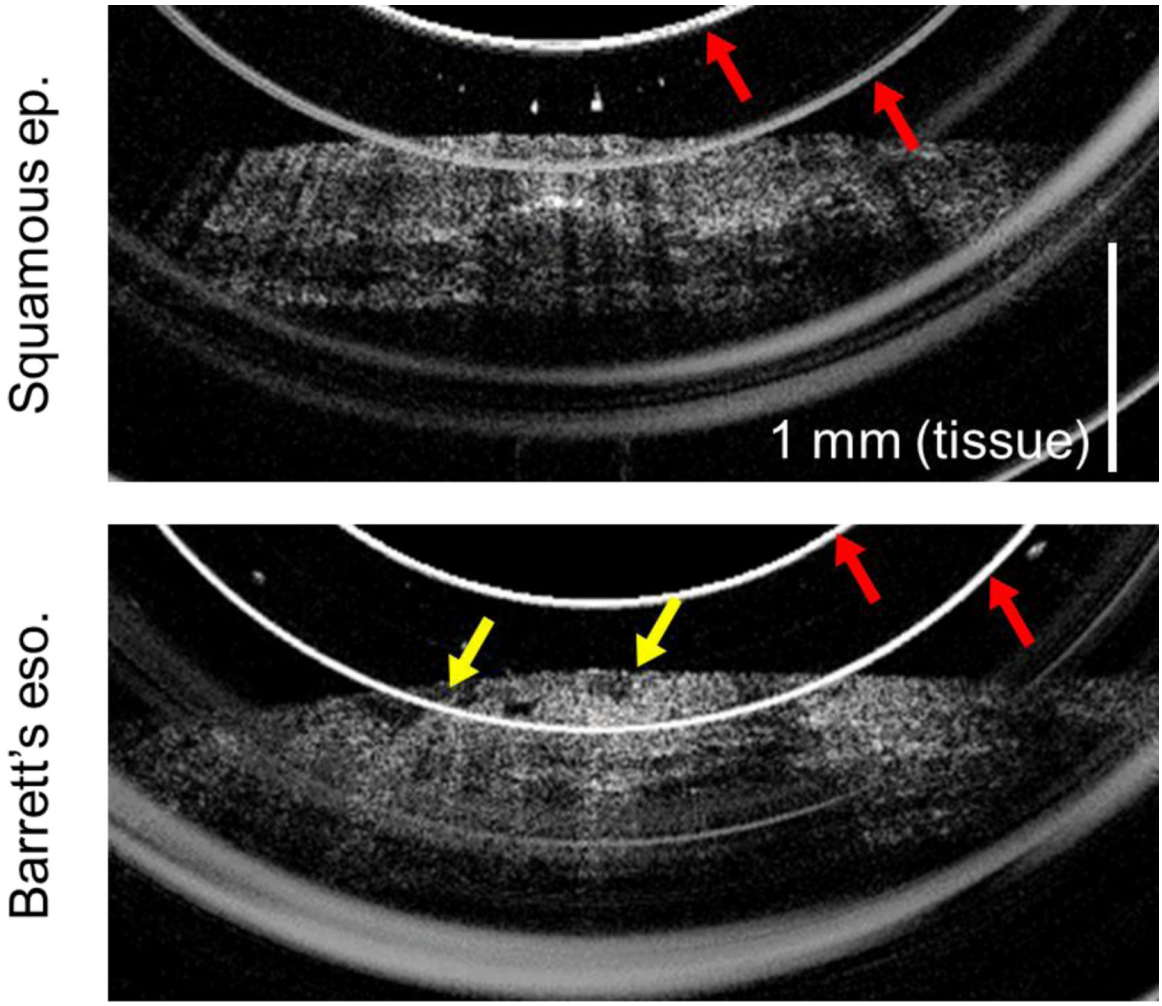

Figure 4:
OCT cross-sectional images of esophageal epithelium acquired by probe version 1. Red arrows indicate artifacts caused by internal probe reflections. Top: Squamous epithelium, showing smooth epithelial surface and consistent layered appearance. Bottom: Barrett's esophagus, exhibiting an uneven nodular surface (yellow arrows).

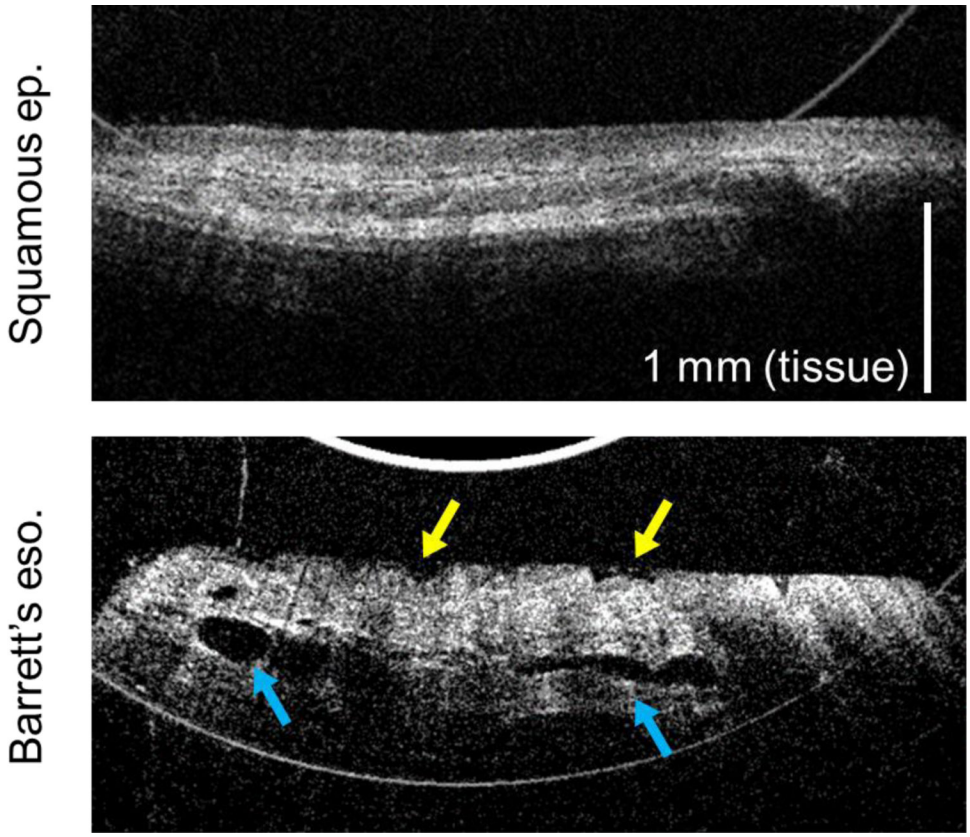

Figure 5:
OCT cross-sectional images of esophageal epithelium acquired by probe version 2, showing substantial decrease in bright ring artifacts. Top: Squamous epithelium, showing smooth epithelial surface and consistent layered appearance. Bottom: Barrett's esophagus, exhibiting an uneven nodular surface (yellow arrows) and ducts from esophageal glands (blue arrows).

Table 1:

Patient enrollment summary

Category	Successfully passaged	Successfully imaged
Total number	37	30
Male	32	28
Female	5	2
Mean age	65.5 years	65.2 years
Age range	24 – 80 years	24 – 78 years
No current BE	28	23
Current BE	9	7
Non-dysplastic BE or indefinite for dysplasia	8	6
Dysplastic BE	1	1
Length of BE (Mean ± SD)	5.1 ± 3.7 cm	5.6 ± 3.9 cm

Table 2:

Number of images classified Barrett's vs. non-Barrett's by OCT image vs. clinical diagnosis

	Clinical: Barrett's	Clinical: Non-Barrett's
OCT: Barrett's	11	4
OCT: Non-Barrett's	2	54